Kennesaw State University

DigitalCommons@Kennesaw State University

1-2017

Search for the 0^{--} glueball in Υ(1S) and Υ(2S) decays

S. Jia et al.
Belle Collaboration

D. Joffe
Kennesaw State University, djoffe@kennesaw.edu

Ratnappuli L. Kulasiri
Kennesaw State University, rkulasir@kennesaw.edu

Search for the 0^{--} glueball in Υ(1S) and Υ(2S) decays

S. Jia *et al.* (Belle Collaboration)

Search for the 0^{--} Glueball in $\Upsilon(1S)$ and $\Upsilon(2S)$ decays

S. Jia,[2] C. P. Shen,[2] C. Z. Yuan,[21] I. Adachi,[15, 11] H. Aihara,[72] S. Al Said,[65, 31] D. M. Asner,[56]

T. Aushev,[45] R. Ayad,[65] V. Babu,[66] I. Badhrees,[65, 30] A. M. Bakich,[64] V. Bansal,[56] E. Barberio,[42]

P. Behera,[20] B. Bhuyan,[19] J. Biswal,[26] G. Bonvicini,[77] A. Bozek,[52] M. Bračko,[40, 26]

T. E. Browder,[14] D. Červenkov,[4] P. Chang,[51] V. Chekelian,[41] A. Chen,[49] B. G. Cheon,[13]

K. Chilikin,[37, 44] K. Cho,[32] S.-K. Choi,[12] Y. Choi,[63] D. Cinabro,[77] N. Dash,[18] S. Di Carlo,[77]

Z. Doležal,[4] Z. Drásal,[4] D. Dutta,[66] S. Eidelman,[3, 55] H. Farhat,[77] J. E. Fast,[56] T. Ferber,[7]

B. G. Fulsom,[56] V. Gaur,[66] N. Gabyshev,[3, 55] A. Garmash,[3, 55] R. Gillard,[77] P. Goldenzweig,[28]

B. Golob,[38, 26] J. Haba,[15, 11] T. Hara,[15, 11] K. Hayasaka,[54] H. Hayashii,[48] M. T. Hedges,[14]

W.-S. Hou,[51] T. Iijima,[47, 46] K. Inami,[46] G. Inguglia,[7] A. Ishikawa,[70] R. Itoh,[15, 11] I. Jaegle,[8]

D. Joffe,[29] K. K. Joo,[5] T. Julius,[42] K. H. Kang,[35] P. Katrenko,[45, 37] T. Kawasaki,[54] H. Kichimi,[15]

C. Kiesling,[41] D. Y. Kim,[61] H. J. Kim,[35] J. B. Kim,[33] K. T. Kim,[33] M. J. Kim,[35] S. H. Kim,[13]

Y. J. Kim,[32] P. Kodyš,[4] S. Korpar,[40, 26] D. Kotchetkov,[14] P. Križan,[38, 26] P. Krokovny,[3, 55]

T. Kuhr,[39] R. Kulasiri,[29] A. Kuzmin,[3, 55] Y.-J. Kwon,[79] J. S. Lange,[9] C. H. Li,[42] L. Li,[59] Y. Li,[76]

L. Li Gioi,[41] J. Libby,[20] D. Liventsev,[76, 15] M. Lubej,[26] T. Luo,[57] M. Masuda,[71] T. Matsuda,[43]

D. Matvienko,[3, 55] K. Miyabayashi,[48] H. Miyata,[54] R. Mizuk,[37, 44, 45] H. K. Moon,[33]

T. Mori,[46] M. Nakao,[15, 11] T. Nanut,[26] K. J. Nath,[19] Z. Natkaniec,[52] M. Nayak,[77, 15]

M. Niiyama,[34] N. K. Nisar,[57] S. Nishida,[15, 11] S. Ogawa,[69] S. Okuno,[27] H. Ono,[53, 54]

Y. Onuki,[72] W. Ostrowicz,[52] G. Pakhlova,[37, 45] B. Pal,[6] C.-S. Park,[79] H. Park,[35] R. Pestotnik,[26]

L. E. Piilonen,[76] C. Pulvermacher,[15] M. Ritter,[39] A. Rostomyan,[7] Y. Sakai,[15, 11] S. Sandilya,[6]

L. Santelj,[15] T. Sanuki,[70] V. Savinov,[57] O. Schneider,[36] G. Schnell,[1, 17] C. Schwanda,[22]

Y. Seino,[54] K. Senyo,[78] M. E. Sevior,[42] V. Shebalin,[3, 55] T.-A. Shibata,[73] J.-G. Shiu,[51]

B. Shwartz,[3, 55] F. Simon,[41, 67] A. Sokolov,[23] E. Solovieva,[37, 45] M. Starič,[26] J. F. Strube,[56]

M. Sumihama,[10] T. Sumiyoshi,[74] K. Suzuki,[62] M. Takizawa,[60, 16, 58] U. Tamponi,[24, 75]

K. Tanida,[25] F. Tenchini,[42] M. Uchida,[73] T. Uglov,[37, 45] Y. Unno,[13] S. Uno,[15, 11] P. Urquijo,[42]

Y. Usov,[3, 55] C. Van Hulse,[1] G. Varner,[14] V. Vorobyev,[3, 55] C. H. Wang,[50] M.-Z. Wang,[51]

P. Wang,[21] Y. Watanabe,[27] E. Widmann,[62] E. Won,[33] Y. Yamashita,[53] H. Ye,[7] J. Yelton,[8]

Z. P. Zhang,[59] V. Zhilich,[3, 55] V. Zhukova,[44] V. Zhulanov,[3, 55] and A. Zupanc[38, 26]

(The Belle Collaboration)

[1]University of the Basque Country UPV/EHU, 48080 Bilbao

[2]Beihang University, Beijing 100191

[3]Budker Institute of Nuclear Physics SB RAS, Novosibirsk 630090

[4]Faculty of Mathematics and Physics, Charles University, 121 16 Prague

[5]Chonnam National University, Kwangju 660-701

[6]University of Cincinnati, Cincinnati, Ohio 45221

[7]Deutsches Elektronen–Synchrotron, 22607 Hamburg

[8]University of Florida, Gainesville, Florida 32611

[9]Justus-Liebig-Universität Gießen, 35392 Gießen

[10]Gifu University, Gifu 501-1193

[11]SOKENDAI (The Graduate University for Advanced Studies), Hayama 240-0193

[12]Gyeongsang National University, Chinju 660-701

[13]Hanyang University, Seoul 133-791

[14]University of Hawaii, Honolulu, Hawaii 96822

[15]High Energy Accelerator Research Organization (KEK), Tsukuba 305-0801

[16]J-PARC Branch, KEK Theory Center,
High Energy Accelerator Research Organization (KEK), Tsukuba 305-0801

[17]IKERBASQUE, Basque Foundation for Science, 48013 Bilbao

[18]Indian Institute of Technology Bhubaneswar, Satya Nagar 751007

[19]Indian Institute of Technology Guwahati, Assam 781039

[20]Indian Institute of Technology Madras, Chennai 600036

[21]Institute of High Energy Physics, Chinese Academy of Sciences, Beijing 100049

[22]Institute of High Energy Physics, Vienna 1050

[23]Institute for High Energy Physics, Protvino 142281

[24]INFN - Sezione di Torino, 10125 Torino

[25]Advanced Science Research Center, Japan Atomic Energy Agency, Naka 319-1195

[26]*J. Stefan Institute, 1000 Ljubljana*

[27]*Kanagawa University, Yokohama 221-8686*

[28]*Institut für Experimentelle Kernphysik,*
Karlsruher Institut für Technologie, 76131 Karlsruhe

[29]*Kennesaw State University, Kennesaw, Georgia 30144*

[30]*King Abdulaziz City for Science and Technology, Riyadh 11442*

[31]*Department of Physics, Faculty of Science,*
King Abdulaziz University, Jeddah 21589

[32]*Korea Institute of Science and Technology Information, Daejeon 305-806*

[33]*Korea University, Seoul 136-713*

[34]*Kyoto University, Kyoto 606-8502*

[35]*Kyungpook National University, Daegu 702-701*

[36]*École Polytechnique Fédérale de Lausanne (EPFL), Lausanne 1015*

[37]*P.N. Lebedev Physical Institute of the Russian Academy of Sciences, Moscow 119991*

[38]*Faculty of Mathematics and Physics,*
University of Ljubljana, 1000 Ljubljana

[39]*Ludwig Maximilians University, 80539 Munich*

[40]*University of Maribor, 2000 Maribor*

[41]*Max-Planck-Institut für Physik, 80805 München*

[42]*School of Physics, University of Melbourne, Victoria 3010*

[43]*University of Miyazaki, Miyazaki 889-2192*

[44]*Moscow Physical Engineering Institute, Moscow 115409*

[45]*Moscow Institute of Physics and Technology, Moscow Region 141700*

[46]*Graduate School of Science, Nagoya University, Nagoya 464-8602*

[47]*Kobayashi-Maskawa Institute, Nagoya University, Nagoya 464-8602*

[48]*Nara Women's University, Nara 630-8506*

[49]*National Central University, Chung-li 32054*

[50]National United University, Miao Li 36003

[51]Department of Physics, National Taiwan University, Taipei 10617

[52]H. Niewodniczanski Institute of Nuclear Physics, Krakow 31-342

[53]Nippon Dental University, Niigata 951-8580

[54]Niigata University, Niigata 950-2181

[55]Novosibirsk State University, Novosibirsk 630090

[56]Pacific Northwest National Laboratory, Richland, Washington 99352

[57]University of Pittsburgh, Pittsburgh, Pennsylvania 15260

[58]Theoretical Research Division, Nishina Center, RIKEN, Saitama 351-0198

[59]University of Science and Technology of China, Hefei 230026

[60]Showa Pharmaceutical University, Tokyo 194-8543

[61]Soongsil University, Seoul 156-743

[62]Stefan Meyer Institute for Subatomic Physics, Vienna 1090

[63]Sungkyunkwan University, Suwon 440-746

[64]School of Physics, University of Sydney, New South Wales 2006

[65]Department of Physics, Faculty of Science, University of Tabuk, Tabuk 71451

[66]Tata Institute of Fundamental Research, Mumbai 400005

[67]Excellence Cluster Universe, Technische Universität München, 85748 Garching

[68]Department of Physics, Technische Universität München, 85748 Garching

[69]Toho University, Funabashi 274-8510

[70]Department of Physics, Tohoku University, Sendai 980-8578

[71]Earthquake Research Institute, University of Tokyo, Tokyo 113-0032

[72]Department of Physics, University of Tokyo, Tokyo 113-0033

[73]Tokyo Institute of Technology, Tokyo 152-8550

[74]Tokyo Metropolitan University, Tokyo 192-0397

[75]University of Torino, 10124 Torino

[76]*Virginia Polytechnic Institute and State University, Blacksburg, Virginia 24061*

[77]*Wayne State University, Detroit, Michigan 48202*

[78]*Yamagata University, Yamagata 990-8560*

[79]*Yonsei University, Seoul 120-749*

Abstract

We report the first search for the $J^{PC} = 0^{--}$ glueball in $\Upsilon(1S)$ and $\Upsilon(2S)$ decays with data samples of (102 ± 2) million and (158 ± 4) million events, respectively, collected with the Belle detector. No significant signals are observed in any of the proposed production modes, and the 90% credibility level upper limits on their branching fractions in $\Upsilon(1S)$ and $\Upsilon(2S)$ decays are obtained. The inclusive branching fractions of the $\Upsilon(1S)$ and $\Upsilon(2S)$ decays into final states with a χ_{c1} are measured to be $\mathcal{B}(\Upsilon(1S) \to \chi_{c1} + anything) = (1.90 \pm 0.43(stat.) \pm 0.14(syst.)) \times 10^{-4}$ with an improved precision over prior measurements and $\mathcal{B}(\Upsilon(2S) \to \chi_{c1} + anything) = (2.24 \pm 0.44(stat.) \pm 0.20(syst.)) \times 10^{-4}$ for the first time.

I. INTRODUCTION

The existence of bound states of gluons (so-called "glueballs"), with a rich spectroscopy and a complex phenomenology, is one of the early predictions of the non-abelian nature of strong interactions described by quantum chromodynamics (QCD) [1]. However, despite many years of experimental efforts, none of these gluonic states have been established unambiguously. Possible reasons for this include the mixing between glueballs and conventional mesons, the lack of solid information on the glueball production mechanism, and the lack of knowledge about glueball decay properties.

Of these difficulties, from the experimental point of view, the most outstanding obstacle is the isolation of glueballs from various quarkonium states. Fortunately, there is a class of glueballs with three gluons and quantum numbers incompatible with quark-antiquark bound states, called oddballs, that are free of this conundrum. The quantum numbers of such glueballs include J^{PC} = 0^{--}, 0^{+-}, 1^{-+}, 2^{+-}, 3^{-+}, and so on. Among oddballs, special attention should be paid to the 0^{--} state (G_{0--}), since it is relatively light and can be produced in the decays of vector quarkonium or quarkoniumlike states. Two 0^{--} oddballs are predicted using QCD sum rules [2] with masses of (3.81 ± 0.12) GeV/c^2 and (4.33 ± 0.13) GeV/c^2, while the lowest-lying state calculated using distinct bottom-up holographic models of QCD [3] has a mass of 2.80 GeV/c^2. Although the masses have been calculated, the width and hadronic couplings to any final states remain unknown. Possible G_{0--} production modes from bottomonium decays are suggested in Ref. [2] including $\Upsilon(1S, 2S) \to \chi_{c1} + G_{0--}$, $\Upsilon(1S, 2S) \to f_1(1285) + G_{0--}$, $\chi_{b1} \to J/\psi + G_{0--}$, and $\chi_{b1} \to \omega + G_{0--}$.

In this paper, we search for 0^{--} glueballs in the production modes proposed above and define $G(2800)$, $G(3810)$, and $G(4330)$ as the glueballs with masses fixed at 2.800, 3.810, and 4.330 GeV/c^2, respectively. All the parent particles in the above processes are copiously produced in the Belle experiment, and may decay to the oddballs with modest rates. Since the widths are unknown, we report an investigation of the 0^{--} glueballs with different assumed widths. The χ_{c1} is reconstructed via its decays into $\gamma J/\psi$, $J/\psi \to \ell^+\ell^-$ and $\ell = e$ or μ, $f_1(1285)$ via $\eta\pi^+\pi^-$ with $\eta \to \gamma\gamma$, and ω via $\pi^+\pi^-\pi^0$ with $\pi^0 \to \gamma\gamma$. As the χ_{c1} are observed clearly as tagged signals in $\Upsilon(1S, 2S)$ decays, the corresponding production rates may be measured with improved precision.

6

II. THE DATA SAMPLE AND BELLE DETECTOR

This analysis utilizes the $\Upsilon(1S)$ and $\Upsilon(2S)$ data samples with a total luminosity of 5.74 and 24.91 fb^{-1}, respectively, corresponding to 102×10^6 $\Upsilon(1S)$ and 158×10^6 $\Upsilon(2S)$ events [4]. An 89.45 fb^{-1} data sample collected at $\sqrt{s} = 10.52$ GeV is used to estimate the possible irreducible continuum contributions. Here, $\sqrt{s}$ is the center-of-mass (C.M.) energy of the colliding e^+e^- system. The data were collected with the Belle detector [5, 6] operated at the KEKB asymmetric-energy e^+e^- collider [7, 8]. Large Monte Carlo (MC) samples of all of the investigated glueball modes are generated with EVTGEN [9] to determine signal line-shapes and efficiencies. The angular distribution for $\Upsilon(2S) \to \gamma\chi_{b1}$ is simulated assuming a pure $E1$ transition ($dN/d\cos\theta_\gamma \propto 1 - \frac{1}{3}\cos^2\theta_\gamma$ [10], where θ_γ is the polar angle of the $\Upsilon(2S)$ radiative photon in the e^+e^- C.M. frame), and uniform phase space is used for the χ_{b1} decays. We use the uniform phase-space decay model for other decays as well. Note that G_{0--} inclusive decays are modelled using PYTHIA [11]. Inclusive $\Upsilon(1S)$ and $\Upsilon(2S)$ MC samples, produced using PYTHIA with four times the luminosity of the real data, are used to identify possible peaking backgrounds from $\Upsilon(1S)$ and $\Upsilon(2S)$ decays.

The Belle detector is a large solid-angle magnetic spectrometer that consists of a silicon vertex detector, a 50-layer central drift chamber (CDC), an array of aerogel threshold Cherenkov counters (ACC), a barrel-like arrangement of time-of-flight scintillation counters (TOF), and an electromagnetic calorimeter comprised of CsI(Tl) crystals (ECL) located inside a superconducting solenoid coil that provides a 1.5 T magnetic field. An iron flux-return yoke located outside the coil is used to detect K_L^0 mesons and to identify muons. A detailed description of the Belle detector can be found in Refs. [5, 6].

III. EVENT SELECTION

Charged tracks from the primary vertex with $dr < 0.5$ cm and $|dz| < 4$ cm are selected, where dr and dz are the impact parameters perpendicular to and along the beam direction, respectively, with respect to the interaction point. In addition, the transverse momentum of every charged track in the laboratory frame is restricted to be larger than 0.1 GeV/c. We require the number of well-reconstructed charged tracks to be greater than four to suppress the significant background from quantum electrodynamics processes. For charged tracks, information from different detector sub-

systems including specific ionization in the CDC, time measurements in the TOF and the response of the ACC is combined to form the likelihood $\mathcal{L}_i$ for particle species i, where $i = \pi, K$, or p [12]. Charged tracks with $R_K = \mathcal{L}_K/(\mathcal{L}_K + \mathcal{L}_\pi) < 0.4$ are considered to be pions. With this condition, the pion identification efficiency is 96% and the kaon misidentification rate is about 9%. A similar likelihood ratio is defined as $R_e = \mathcal{L}_e/(\mathcal{L}_e + \mathcal{L}_{\mathrm{non}-e})$ [13] for electron identification and $R_\mu = \mathcal{L}_\mu/(\mathcal{L}_\mu + \mathcal{L}_K + \mathcal{L}_\pi)$ [14] for muon identification. An ECL cluster is taken as a photon candidate if it does not match the extrapolation of any charged track and its energy is greater than 50 MeV.

To reduce the effect of bremsstrahlung and final-state radiation, photons detected in the ECL within a 50 mrad cone of the original electron or positron direction are included in the calculation of the e^+/e^- four-momentum. For the lepton pair $\ell^+\ell^-$ used to reconstruct the J/ψ, both of the tracks should have $R_e > 0.95$ in the e^+e^- mode; or one track should have $R_\mu > 0.95$ and the other $R_\mu > 0.05$ in the $\mu^+\mu^-$ mode. The lepton pair identification efficiencies for e^+e^- and $\mu^+\mu^-$ are 96% and 93%, respectively. After all event selection requirements, significant J/ψ signals are seen in the $\Upsilon(1S)$ and $\Upsilon(2S)$ data samples, as shown in Figs. 1 (a) and (b). Since different modes have almost the same J/ψ mass resolutions, we define the J/ψ signal region in the window $|M_{\ell^+\ell^-} - m_{J/\psi}| < 0.03$ GeV/c^2 ($\sim 2.5\sigma$) indicated by the arrows, where $m_{J/\psi}$ is the J/ψ nominal mass [15], while the J/ψ mass sideband is 2.97 GeV/$c^2 < M_{\ell^+\ell^-} < 3.03$ GeV/c^2 or 3.17 GeV/$c^2 < M_{\ell^+\ell^-} < 3.23$ GeV/c^2, which is twice as wide as the signal region. In order to improve the J/ψ momentum resolution, a mass-constrained fit is applied to the J/ψ candidates in the signal region.

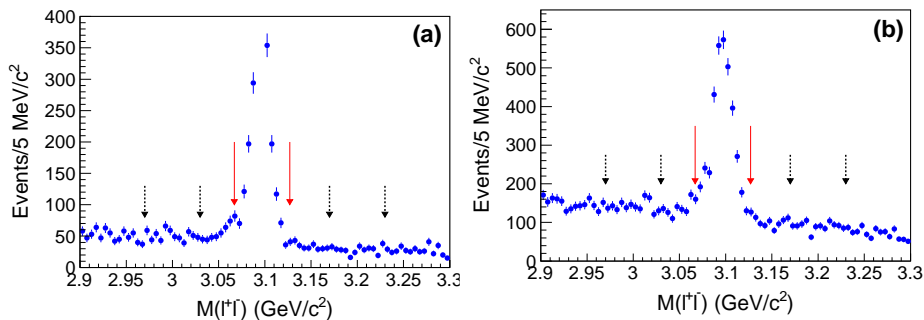FIG. 1: The $\ell^+\ell^-$ invariant mass distributions in the $\Upsilon(1S)$ (a) and $\Upsilon(2S)$ (b) data samples. The solid arrows show the J/ψ signal region, and the dashed arrows show the J/ψ mass sideband regions.

8

IV. MEASUREMENTS OF $\Upsilon(1S, 2S) \to \chi_{\mathbf{c1}} + \mathbf{anything}$

Before searching for the G_{0--} in $\Upsilon(1S, 2S) \to \chi_{c1} + G_{0--}$, we measure the inclusive χ_{c1} production in $\Upsilon(1S, 2S)$. The J/ψ candidate is combined with any one of the photon candidates to reconstruct the χ_{c1} signal. The $\gamma J/\psi$ invariant mass distributions for the χ_{c1} candidates are shown in Figs. 2(a) and 3(a) from $\Upsilon(1S)$ and $\Upsilon(2S)$ decays, respectively. Clear χ_{c1} signals are observed in both data samples, while no clear χ_{c2} signals are seen. No evidence for χ_{c1} signals is found in the J/ψ-mass sideband events nor the continuum data sample, as can be seen from the same plots.
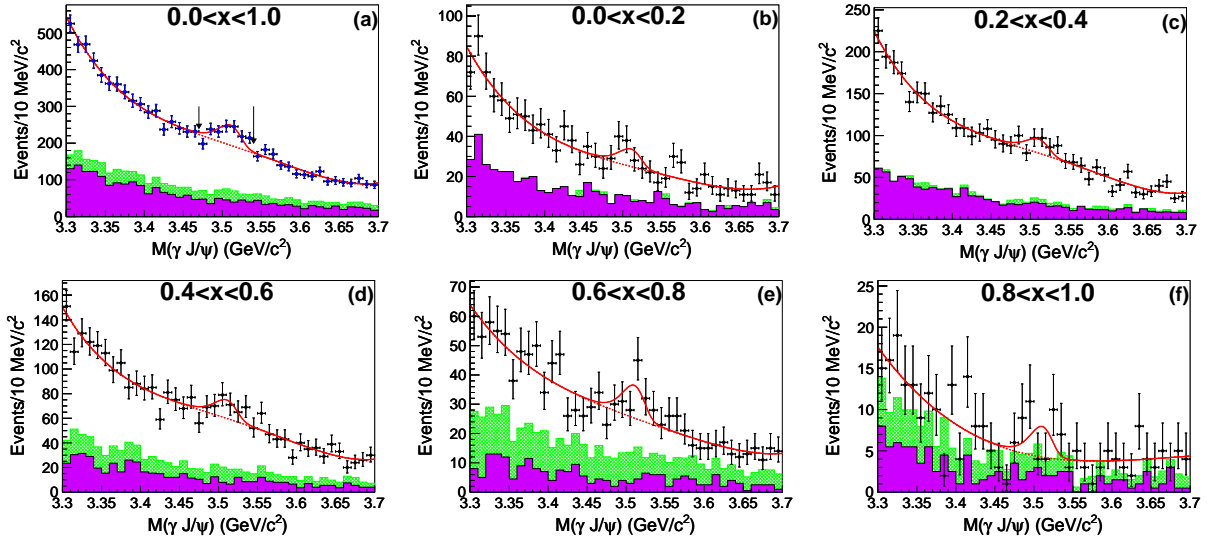

FIG. 2: (Color online) Invariant mass distributions of the χ_{c1} candidates in the entire x region (a) and for x bins of size 0.2 (b–f). The dots with error bars are the $\Upsilon(1S)$ data. The solid lines are the best fits, and the dotted lines represent the backgrounds. The shaded histograms are from the normalized J/ψ mass sidebands and cross-hatched histograms are from the normalized continuum contributions described in the text. The arrows in (a) show the χ_{c1} signal region that will be used to search for glueballs in the channel $\Upsilon(1S) \to \chi_{c1} + G_{0--}$ below.

The continuum background contribution is determined using a large amount of data taken at $\sqrt{s} = 10.52$ GeV, extrapolated down to the lower resonances. The scale factor used for this extrapolation is $f_{\text{scale}} = \mathcal{L}_\Upsilon/\mathcal{L}_{\text{con}} \times \sigma_\Upsilon/\sigma_{\text{con}} \times \varepsilon_\Upsilon/\varepsilon_{\text{con}}$, where $\mathcal{L}_\Upsilon/\mathcal{L}_{\text{con}}$, $\sigma_\Upsilon/\sigma_{\text{con}}$, and $\varepsilon_\Upsilon/\varepsilon_{\text{con}}$ are the ratios of the integrated luminosities, cross sections, and efficiencies, respectively, for the Υ and continuum samples. The cross section extrapolation with beam energy is assumed to have a $1/s^2$ [16–18] dependence. Contributions from e^+e^- annihilation without J/ψ events have been
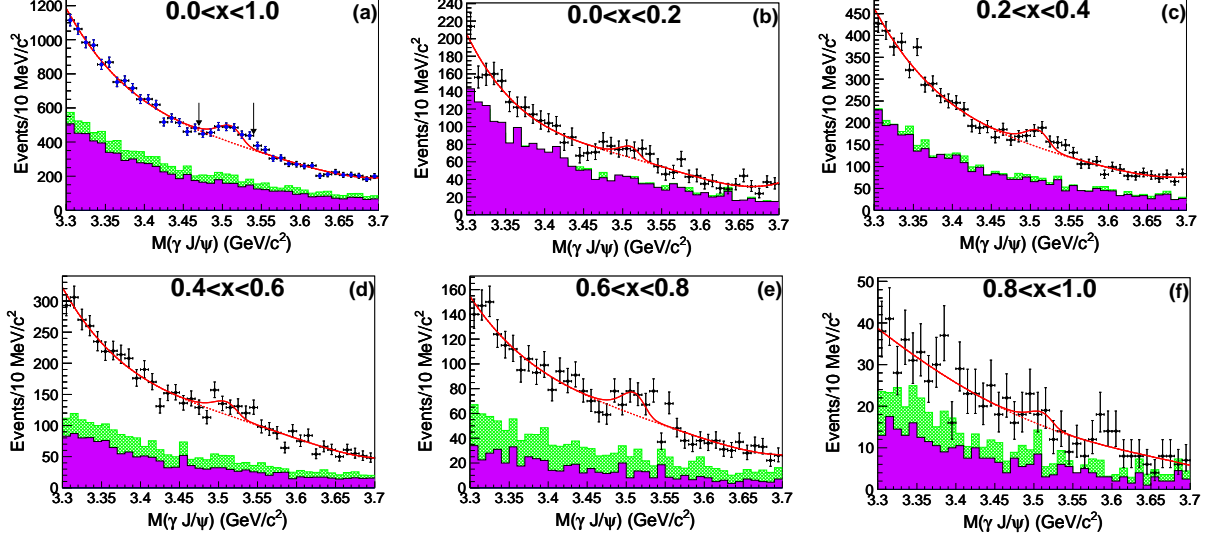
9

FIG. 3: (Color online) Invariant mass distributions of the χ_{c1} candidates in the entire x region (a) and for x bins of size 0.2 (b–f). The dots with error bars are the $\Upsilon(2S)$ data. The solid lines are the best fits, and the dotted lines represent the backgrounds. The shaded histograms are from the normalized J/ψ mass sidebands and cross-hatched histograms are from the normalized continuum contributions described in the text. The arrows in (a) show the χ_{c1} signal region that will be used to search for glueballs in the channel $\Upsilon(2S) \to \chi_{c1} + G_{0--}$ below.

subtracted to avoid double counting of continuum events. The resulting scale factor is about 0.10 for $\Upsilon(1S)$ and 0.35 for $\Upsilon(2S)$ decays. For $\Upsilon(2S) \to \chi_{c1} + anything$, another background is the intermediate transition $\Upsilon(2S) \to \pi^+\pi^-\Upsilon(1S)$ or $\pi^0\pi^0\Upsilon(1S)$ with $\Upsilon(1S)$ decaying into χ_{c1}. Such contamination is removed by requiring the $\pi\pi$ recoil mass to be outside the $[9.45, 9.47]$ GeV/c^2 region for all $\pi\pi$ combinations.

Considering the slight differences in the MC-determined reconstruction efficiencies for different χ_{c1} momenta, we partition the data samples according to the scaled momentum $x = p^*_{\chi_{c1}}/(\frac{1}{2\sqrt{s}} \times (s - m^2_{\chi_{c1}}))$ [19], where $p^*_{\chi_{c1}}$ is the momentum of the χ_{c1} candidate in the e^+e^- C.M. system, and $m_{\chi_{c1}}$ is the χ_{c1} nominal mass [20]. The value of $\frac{1}{2\sqrt{s}} \times (s - m^2_{\chi_{c1}})$ is the value of $p^*_{\chi_{c1}}$ for the case where the χ_{c1} candidate recoils against a massless particle. The use of x removes the beam-energy dependence in comparing the continuum data to that taken at the $\Upsilon(1S, 2S)$ resonances. The $\gamma J/\psi$ invariant mass distribution in each $\Delta x = 0.2$ bin is shown in Figs. 2(b–f) and 3(b–f) for $\Upsilon(1S)$ and $\Upsilon(2S)$ decays, respectively.

An unbinned extended likelihood fit is applied to the x-dependent χ_{c1} spectra to extract the signal yields in the $\Upsilon(1S)$ or $\Upsilon(2S)$ data sample. Due to the slight dependence on momentum, the

χ_{c1} shape in each x bin is described by a Breit-Wigner (BW) function convolved with a Novosibirsk function [21], where all parameter values are fixed to those from the fit to the MC-simulated χ_{c1} signal. Since no peaking backgrounds are found, a third-order Chebyshev polynomial shape is used for the backgrounds. The fit results are shown in Figs. 2 and 3, and the fitted χ_{c1} signal yields (N_{fit}) in the entire x region and each x bin from $\Upsilon(1S)$ and $\Upsilon(2S)$ decays are itemized in Table I, together with the reconstruction efficiencies from MC signal simulations (ε), the total systematic uncertainties (σ_{syst})—which are the sum of the common systematic errors (discussed below)—and fit errors estimated in each x bin or the full range in x, and the corresponding branching fractions ($\mathcal{B}$). The total numbers of χ_{c1} events, *i.e.*, the sums of the signal yields in all of the x bins, the sums of the x-dependent efficiencies weighted by the signal fraction in that x bin, and the measured branching fractions are listed in the bottom row. In comparison with the previous result of $(2.3 \pm 0.7) \times 10^{-4}$ [19] for $\Upsilon(1S) \to \chi_{c1} + anything$, our measurement of $(1.90 \pm 0.43(stat.) \pm 0.14(syst.)) \times 10^{-4}$ has an improved precision and lower continuum background due to the requirement that the number of charged tracks be greater than four. The branching fraction for $\Upsilon(2S) \to \chi_{c1} + anything$ is measured for the first time and found to be $(2.24 \pm 0.44(stat.) \pm 0.20(syst.)) \times 10^{-4}$. The differential branching fractions of $\Upsilon(1S, 2S)$ decays into χ_{c1} are shown in Fig. 4. A fit with an additional χ_{c2} signal shape is also performed in the entire x region in the $\Upsilon(1S)$ or $\Upsilon(2S)$ data sample, as shown in Fig. 5. The difference in the number of fitted χ_{c1} yields is included in the systematic error. The χ_{c2} signal significance from the fit is less than 2.7σ (3.2σ) in the $\Upsilon(1S)$ ($\Upsilon(2S)$) data sample. The 90% credibility level (C.L.) [22] upper limit (measured as described below) for the $\Upsilon(1S) \to \chi_{c2} + anything$ branching fraction is 3.09×10^{-4}, with systematic errors included, to be compared with the previous result of $(3.4 \pm 1.0) \times 10^{-4}$ [19], and the measured $\Upsilon(2S) \to \chi_{c2} + anything$ branching fraction is $(2.28 \pm 0.73(stat.) \pm 0.34(syst.)) \times 10^{-4}$ ($< 3.28 \times 10^{-4}$ at 90% C.L.).

V.   SEARCH FOR 0^{--} GLUEBALLS IN $\Upsilon(1S)$, $\Upsilon(2S)$, AND χ_{b1} DECAYS

In the channels $\Upsilon(1S, 2S) \to \chi_{c1} + G_{0^{--}}$, $\Upsilon(1S, 2S) \to f_1(1285) + G_{0^{--}}$, $\chi_{b1} \to J/\psi + G_{0^{--}}$, and $\chi_{b1} \to \omega + G_{0^{--}}$, we search for the $G_{0^{--}}$ signals in the recoil mass spectra of the χ_{c1}, $f_1(1285)$, J/ψ, and ω with $G_{0^{--}}$ widths varying from 0.0 to 0.5 GeV in steps of 0.05 GeV. After all selection requirements, no peaking backgrounds are found in the χ_{c1}, $f_1(1285)$, J/ψ, or ω mass sideband events, or in the continuum production in the $G_{0^{--}}$ signal regions, in agreement with the

11

TABLE I: Summary of the branching fraction measurements of $\Upsilon(1S, 2S)$ inclusive decays into χ_{c1}, where N_{fit} is the number of fitted signal events, ε (%) is the reconstruction efficiency, σ_{syst} (%) is the total systematic error on the branching fraction measurement, and $\mathcal{B}$ is the measured branching fraction.

|	$\Upsilon(1S) \to \chi_{c1}$ + anything				$\Upsilon(2S) \to \chi_{c1}$ + anything			
x	N_{fit}	$\varepsilon(\%)$	$\sigma_{\text{syst}}(\%)$	$\mathcal{B}(10^{-4})$	N_{fit}	$\varepsilon(\%)$	$\sigma_{\text{syst}}(\%)$	$\mathcal{B}(10^{-4})$
$(0.0, 0.2)$	34.0 ± 18.0	31.77	17.0	$0.25 \pm 0.13 \pm 0.04$	43.0 ± 25.1	30.56	15.6	$0.22 \pm 0.13 \pm 0.03$
$(0.2, 0.4)$	65.2 ± 30.7	29.09	7.2	$0.53 \pm 0.25 \pm 0.04$	161.3 ± 44.1	27.11	9.6	$0.93 \pm 0.25 \pm 0.09$
$(0.4, 0.6)$	58.4 ± 26.9	27.70	9.5	$0.50 \pm 0.23 \pm 0.05$	85.5 ± 39.0	26.50	9.6	$0.49 \pm 0.22 \pm 0.05$
$(0.6, 0.8)$	43.4 ± 18.3	25.72	13.0	$0.40 \pm 0.17 \pm 0.05$	72.7 ± 28.5	24.25	12.6	$0.47 \pm 0.18 \pm 0.06$
$(0.8, 1.0)$	14.4 ± 9.5	15.35	22.3	$0.22 \pm 0.15 \pm 0.05$	13.1 ± 14.2	15.69	17.4	$0.13 \pm 0.14 \pm 0.02$
All x	215.4 ± 49.2	27.54	7.1	$1.90 \pm 0.43 \pm 0.14$	375.6 ± 73.2	26.41	9.1	$2.24 \pm 0.44 \pm 0.20$
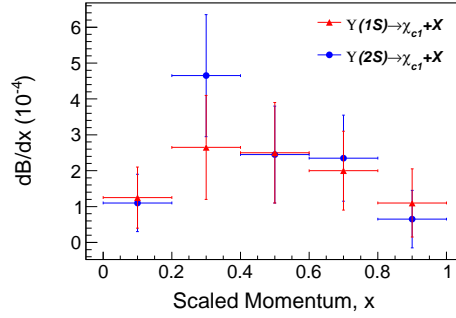
FIG. 4: Differential branching fractions for $\Upsilon(1S)$ and $\Upsilon(2S)$ inclusive decays into χ_{c1} as a function of the scaled momentum x, defined in the text. The error bar of each point is the sum in quadratic of the statistical and systematic errors.

expectation according to the $\Upsilon(1S, 2S)$ generic MC samples.

An unbinned extended maximum-likelihood fit to all the recoil mass spectra is performed to extract the signal and background yields in the $\Upsilon(1S)$ and $\Upsilon(2S)$ data samples. The signal shapes of the $G_{0^{--}}$ signals used in the fits are obtained directly from MC simulations, while for the background a third-order Chebyshev polynomial function is adopted. In each fit, only one glueball candidate with fixed mass and width is included and the upper limit on the number of signal events is obtained.
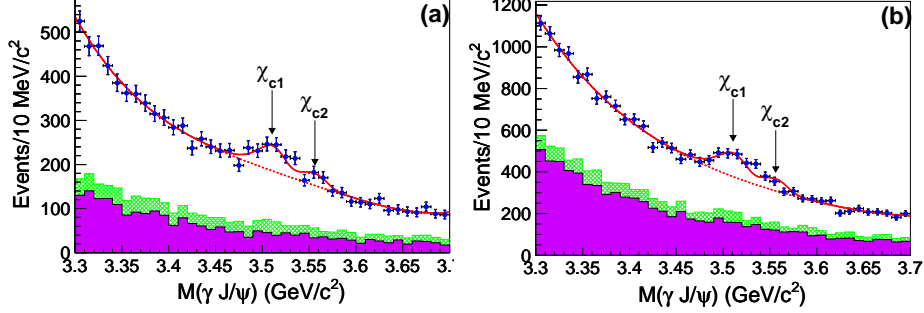
FIG. 5: (Color online) The $\gamma J/\psi$ invariant mass distributions in the entire x region in $\Upsilon(1S)$ (a) and $\Upsilon(2S)$ (b) data. The dots with error bars are the $\Upsilon(1S,2S)$ data. The arrows show the expected positions of the χ_{c1} and χ_{c2} signals. The solid lines are the best fits with the χ_{c1} and χ_{c2} signals included, and the dotted lines represent the backgrounds. The shaded histograms are from the normalized J/ψ mass sidebands and cross-hatched histograms are from the normalized continuum contributions described in the text.

A. MEASUREMENTS OF $\Upsilon(1S,2S) \rightarrow \chi_{c1} + G_{0--}$

For $\Upsilon(1S,2S) \rightarrow \chi_{c1} + G_{0--}$, Figs. 6(a) and (b) show the scatter plots of the $\gamma J/\psi$ recoil mass versus the energy of the photon in the $\gamma J/\psi$ C.M. frame in the $\Upsilon(1S)$ and $\Upsilon(2S)$ data samples, respectively. We require the photon energy from χ_{c1} radiative decays in the $\gamma J/\psi$ C.M. frame to satisfy $0.36\,\mathrm{GeV} < E_\gamma^* < 0.41\,\mathrm{GeV}$ to suppress the non-χ_{c1} backgrounds. The χ_{c1} mass sidebands are defined as $0.25\,\mathrm{GeV} < E_\gamma^* < 0.28\,\mathrm{GeV}$ or $0.43\,\mathrm{GeV} < E_\gamma^* < 0.50\,\mathrm{GeV}$. After the application of the above requirements, Fig. 7 shows the recoil mass spectra of χ_{c1} candidates in the $\Upsilon(1S,2S)$ data. There are no evident signals for any of the G_{0--} states at any of the expected positions. Since the width is unknown, the fit is repeated with G_{0--} widths from 0 to 0.5 GeV in steps of 0.05 GeV. The fit results for the $G(2800)$, $G(3810)$, and $G(4330)$ signals with their widths fixed at 0.15 GeV are shown in Fig. 7 as an example. The fit yields -3.8 ± 3.9 (6.2 ± 6.4), -20.4 ± 7.8 (-18.5 ± 9.2), and -5.7 ± 11.3 (12.5 ± 14.9) events for the $G(2800)$, $G(3810)$, and $G(4330)$ signals, respectively, in the $\Upsilon(1S)$ ($\Upsilon(2S)$) data sample.

Since the statistical significance in each case is less than 3σ, upper limits on the numbers of signal events, N^{UL}, are determined at the 90% C.L. by solving the equation $\int_0^{N^{\mathrm{UL}}} \mathcal{L}(x)dx / \int_0^{+\infty} \mathcal{L}(x)dx = 0.9$, where x is the number of signal events and $\mathcal{L}(x)$ is the maximized likelihood of the data assuming x signal events. The signal significances are calculated using $\sqrt{-2\ln(\mathcal{L}(0)/\mathcal{L}_{\mathrm{max}})}$, where $\mathcal{L}_{\mathrm{max}}$ is the maximum of $\mathcal{L}(x)$. To take into account systematic uncertainties discussed below, the above likelihood is convolved with a Gaussian function whose
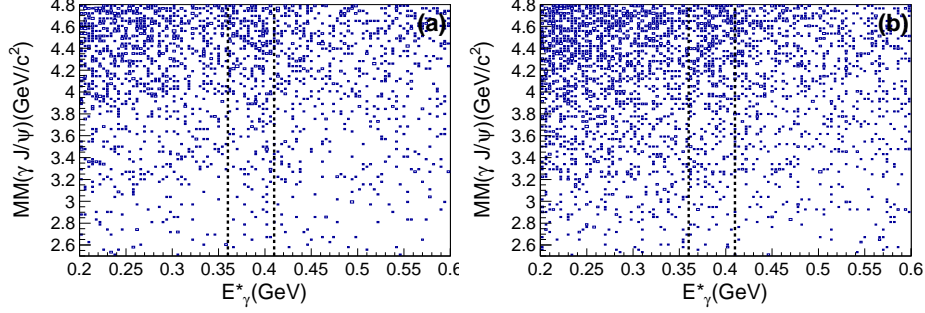
13

FIG. 6: Scatter plots of the recoil mass of $\gamma J/\psi$ versus the photon energy from χ_{c1} radiative decays in the $\gamma J/\psi$ C.M. frame in $\Upsilon(1S)$ (a) and $\Upsilon(2S)$ (b) data. The dotted lines show the expected χ_{c1} signal region.
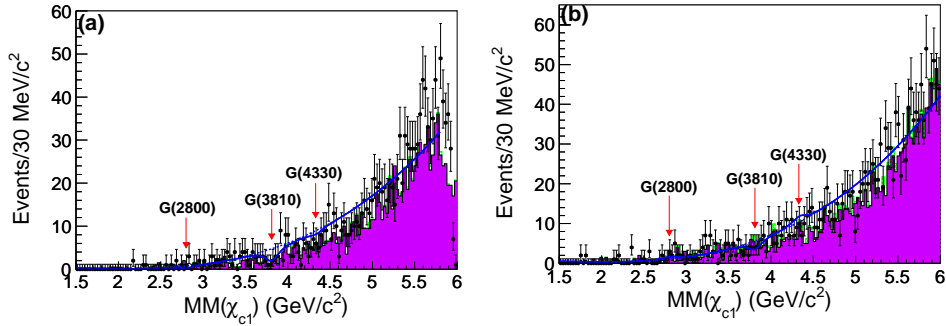

FIG. 7: (Color online) The χ_{c1} recoil mass spectra in the $\Upsilon(1S)$ (a) and $\Upsilon(2S)$ (b) data samples. The solid curves show the results of the fit described in the text, including the $G(2800)$, $G(3810)$, and $G(4330)$ states, with a common width fixed to 0.15 GeV (for illustration) and with central values indicated by the arrows. The dashed curves show the fitted background. The shaded histograms are from the normalized χ_{c1} mass sideband events and the cross-hatched histograms show the normalized continuum contributions.

width equals the total systematic uncertainty.

The calculated upper limits on the numbers of signal events (N^{UL}) and branching fraction ($\mathcal{B}^{\mathrm{UL}}$) with widths from 0.0 to 0.5 GeV for each G_{0--} state are listed in Table II, together with the reconstruction efficiencies (ε) and the systematic uncertainties (σ_{syst}). The results are displayed graphically in Fig. 8.

B. MEASUREMENTS OF $\Upsilon(1S, 2S) \to f_1(1285) + G_{0--}$

Candidate $f_1(1285)$ states are reconstructed via $\eta\pi^+\pi^-$, $\eta \to \gamma\gamma$. The energies of the photons from the η decays are required to be greater than 0.25 GeV to suppress background photons. The photons from possible π^0 decays are vetoed if the invariant mass of one photon from
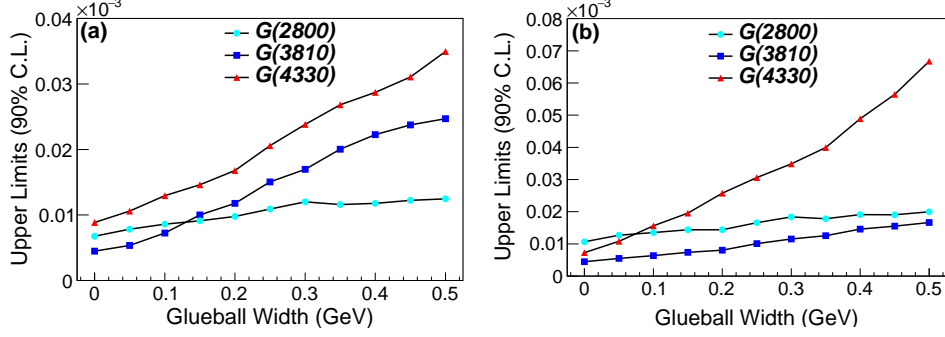
FIG. 8: (Color online) The upper limits on the branching fractions for $\Upsilon(1S) \to \chi_{c1} + G_{0--}$ (a) and $\Upsilon(2S) \to \chi_{c1} + G_{0--}$ (b) as a function of the assumed G_{0--} decay width.

the η candidate and any other photon satisfies $|M(\gamma\gamma) - m_{\pi^0}| < 18$ MeV/c^2, where m_{π^0} is the π^0 nominal mass. We perform a mass-constrained kinematic fit to the surviving η candidates and require $\chi^2 < 10$. A clear K_S^0 signal is seen in the $\pi^+\pi^-$ invariant mass distribution and such backgrounds are removed by requiring that the $\pi^+\pi^-$ mass not fall between 0.475 and 0.515 GeV/c^2. After the application of these requirements, the scatter plots of the $\eta\pi^-$ invariant mass versus the $\eta\pi^+$ invariant mass in $\Upsilon(1S)$ and $\Upsilon(2S)$ data are shown in Figs. 9(a) and (b), respectively; here, $a_0(980)$ signals are observed. Since the $f_1(1285)$ decays into $\eta\pi^+\pi^-$ primarily via the $a_0(980)\pi$ intermediate state, we require either $M(\eta\pi^+)$ or $M(\eta\pi^-)$ to be in a ± 60 MeV/c^2 mass window centered on the $a_0(980)$ nominal mass. The $\eta\pi^+\pi^-$ invariant mass spectra are shown in Fig. 10; clear $f_1(1285)$ and $\eta(1405)$ signals are observed. BW functions are convolved with Novosibirsk functions for the $f_1(1285)$ and $\eta(1405)$ signal shapes and a third-order Chebychev function is taken for the background shape in the fits to the $\eta\pi^+\pi^-$ invariant mass spectra. The fit results are shown in Fig. 10 as the solid lines. We define the $f_1(1285)$ signal region as 1.23 GeV/$c^2 < M(\eta\pi^+\pi^-) < 1.33$ GeV/c^2 and its mass sideband as $1.50\,\mathrm{GeV}/c^2 < M(\eta\pi^+\pi^-) < 1.60\,\mathrm{GeV}/c^2$.

After applying all of the above requirements, Fig. 11 shows the recoil mass spectra of the $f_1(1285)$ in $\Upsilon(1S, 2S)$ data, together with the background from the normalized $f_1(1285)$ mass sideband events and the normalized continuum contributions. No evident G_{0--} signals are seen. An unbinned extended maximum-likelihood fit, repeated with G_{0--} widths from 0 to 0.5 GeV in steps of 0.05 GeV, is applied to the recoil mass spectra. The results of illustrative fits including $G(2800)$, $G(3810)$, and $G(4330)$ signals with widths fixed at 0.15 GeV are shown in Fig. 11. The fits yield 20.2 ± 14.2 (25.0 ± 22.3) $G(2800)$ signal events, -23.0 ± 25.2 (31.7 ± 39.0) $G(3810)$
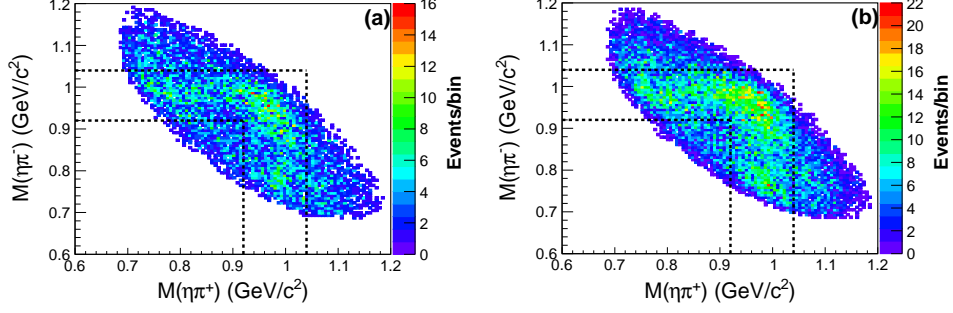
15

FIG. 9: (Color online) Scatter plots of $M(\eta\pi^-)$ versus $M(\eta\pi^+)$ in $\Upsilon(1S)$ (a) and $\Upsilon(2S)$ (b) data. The dotted lines show the $a_0(980)$ signal region.
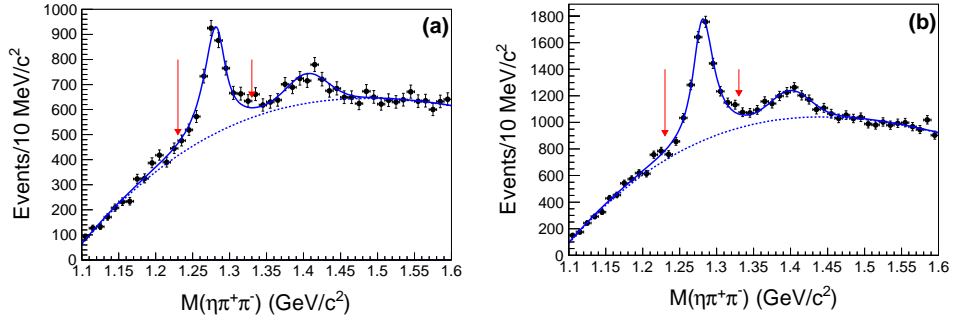

FIG. 10: The $\eta\pi^+\pi^-$ invariant mass spectra in $\Upsilon(1S)$ (a) and $\Upsilon(2S)$ (b) data with the $\eta\pi$ mass within the $a_0(980)$ mass region. The solid lines are the best fits and the dotted lines represent the backgrounds. The red arrows show the $f_1(1285)$ signal region.

signal events, and 31.8 ± 30.0 (68.3 ± 47.2) $G(4330)$ signal events in $\Upsilon(1S)$ ($\Upsilon(2S)$) data.

C. MEASUREMENTS OF $\chi_{b1} \to J/\psi + G_{0--}$

The χ_{b1} is identified through the decay $\Upsilon(2S) \to \gamma\chi_{b1}$. Figure 12 shows the scatter plot of the recoil mass of $\gamma J/\psi$ versus the energy of the $\Upsilon(2S)$ radiative photon in the e^+e^- C.M. frame and the E_γ^* distribution. To select the χ_{b1} signal, we require $0.115\,\text{GeV} < E_\gamma^* < 0.145\,\text{GeV}$. Figure 13 shows the recoil mass spectrum of $\gamma J/\psi$ in $\Upsilon(2S)$ data after all of the above selections, together with the background estimated from the normalized J/ψ mass sideband events and the normalized continuum contributions. No evident G_{0--} signal is observed. An unbinned extended maximum-likelihood fit is applied to the $\gamma J/\psi$ recoil mass spectrum. The result of a typical fit including $G(2800)$, $G(3810)$, and $G(4330)$ signals with widths fixed at 0.15 GeV is shown in Fig. 13. The fit yields -11.4 ± 6.8 $G(2800)$ signal events, -7.1 ± 13.5 $G(3810)$ signal events, and 27.0 ± 19.5
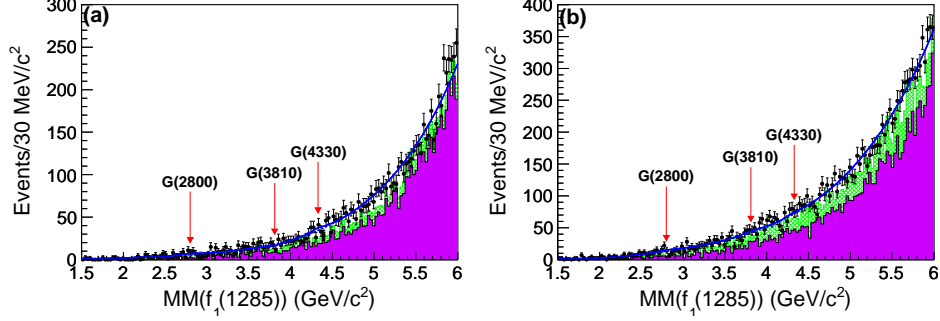
FIG. 11: (Color online) The $f_1(1285)$ recoil mass spectra in the $\Upsilon(1S)$ (a) and $\Upsilon(2S)$ (b) data samples. The solid curves show the results of the fit described in the text, including the $G(2800)$, $G(3810)$, and $G(4330)$ states, with a common width fixed to 0.15 GeV and with central values indicated by the arrows. The dashed curves show the fitted background. The shaded histograms are from the normalized $f_1(1285)$ mass sideband events and the cross-hatched histograms show the normalized continuum contributions.

$G(4330)$ signal events.
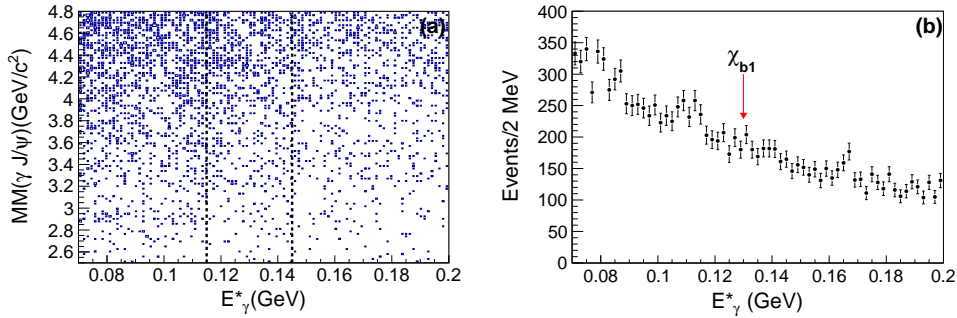
FIG. 12: Scatter plot of the recoil mass of $\gamma J/\psi$ versus the energy of the $\Upsilon(2S)$ radiative photon in the e^+e^- C.M. frame (a) and the distribution of the $\Upsilon(2S)$ radiative photon's energy (b). The dotted lines indicate the expected χ_{b1} signal region. The arrow shows the position of χ_{b1}.

D. MEASUREMENTS OF $\chi_{b1} \to \omega + G_{0^{--}}$

Candidate ω states are reconstructed via $\pi^+\pi^-\pi^0$. We perform a mass-constrained kinematic fit to the selected π^0 candidate and require $\chi^2 < 10$. To remove the backgrounds with K_S^0, the $\pi^+\pi^-$ invariant mass must not lie between 0.475 and 0.515 GeV/c^2. As shown in Fig. 14, a clear ω signal is seen in the $\pi^+\pi^-\pi^0$ invariant mass spectrum in $\Upsilon(2S)$ data. We define the ω signal region as $0.755 \text{ GeV}/c^2 < M(\pi^+\pi^-\pi^0) < 0.805 \text{ GeV}/c^2$ and its mass sideband as $0.820 \text{ GeV}/c^2 < M(\pi^+\pi^-\pi^0) < 0.870 \text{ GeV}/c^2$. Figure 15 shows the scatter plot of the recoil mass
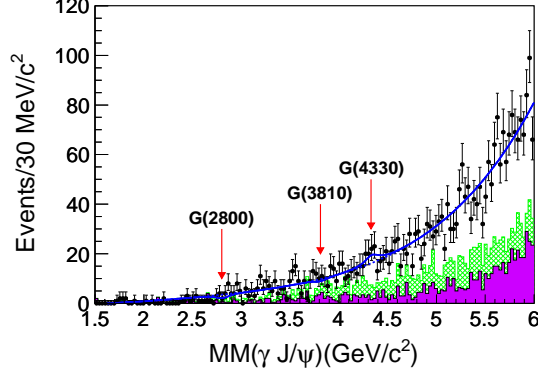
FIG. 13: (Color online) The $\gamma J/\psi$ recoil mass spectrum for $\Upsilon(2S) \to \gamma\chi_{b1} \to \gamma J/\psi + anything$ in the $\Upsilon(2S)$ data sample. The solid curve shows the result of the fit described in the text, including the $G(2800)$, $G(3810)$, and $G(4330)$ states, with a common width fixed to 0.15 GeV and with central values indicated by the arrows. The dashed curve shows the fitted background. The shaded histogram is from the normalized J/ψ mass sideband events and the cross-hatched histogram shows the normalized continuum contributions.

of $\gamma\omega$ versus the energy of the $\Upsilon(2S)$ radiative photon in the e^+e^- C.M. and the distribution of the energy of the $\Upsilon(2S)$ radiative photon. From the plots, no clear χ_{b1} signal is observed. Figure 16 shows the recoil mass spectrum of $\gamma\omega$ for events in the ω signal region, and the background from the normalized ω mass sideband events and from the normalized continuum contributions. No evident G_{0--} signal is observed. An unbinned extended maximum-likelihood fit is applied to the $\gamma\omega$ recoil mass spectrum. The result of a fit including $G(2800)$, $G(3810)$, and $G(4330)$ signals with widths fixed at 0.15 GeV is shown in Fig. 16. The fit yields 22.0 ± 34.1 $G(2800)$, 129.6 ± 75.2 $G(3810)$, and 132.9 ± 364.5 $G(4330)$ signal events.
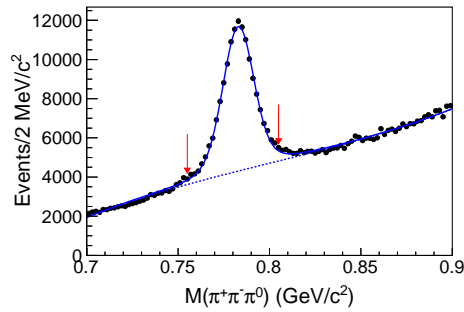

FIG. 14: The $\pi^+\pi^-\pi^0$ invariant mass distribution in $\Upsilon(2S)$ data. The arrows show the ω signal region.

Using the same method as described for $\Upsilon(1S, 2S) \to \chi_{c1} + G_{0--}$, the calculated upper limits on the numbers of signal events (N^{UL}), the reconstruction efficiencies (ε), and the systematic uncertainties (σ_{syst}) for $\Upsilon(1S, 2S) \to f_1(1285) + G_{0--}$, $\chi_{b1} \to J/\psi + G_{0--}$ and $\chi_{b1} \to \omega + G_{0--}$
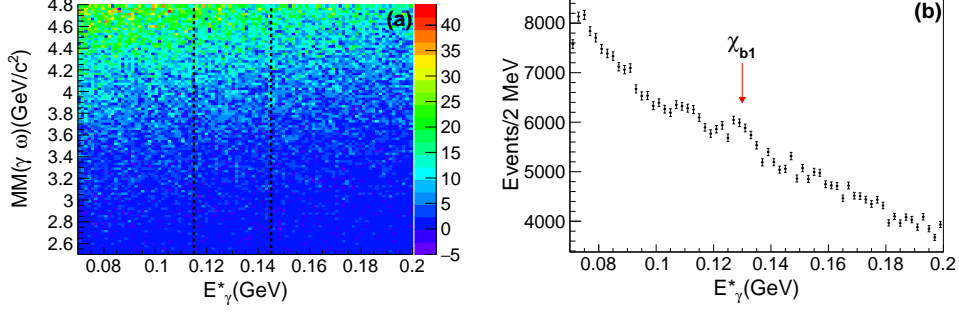
FIG. 15: (Color online) Scatter plot of the recoil mass of $\gamma\omega$ versus the energy of the $\Upsilon(2S)$ radiative photon in the e^+e^- C.M. frame (a) and the distribution of the energy of the $\Upsilon(2S)$ radiative photon (b). The dotted lines in (a) indicate the expected χ_{b1} signal region. The arrow in (b) shows the position of χ_{b1}.
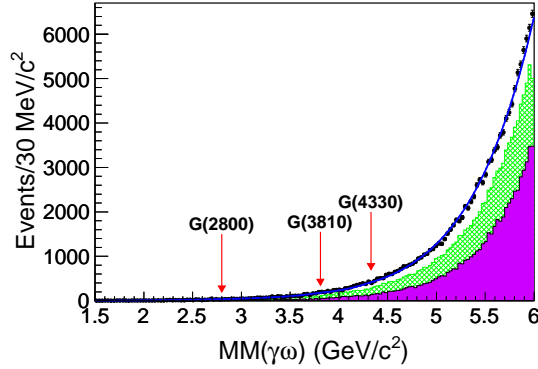

FIG. 16: (Color online) The $\gamma\omega$ recoil mass spectrum for $\Upsilon(2S) \rightarrow \gamma\chi_{b1} \rightarrow \gamma\omega + anything$ in the $\Upsilon(2S)$ data sample. The solid curve shows the result of the fit described in the text, including the $G(2800)$, $G(3810)$, and $G(4330)$ states, with a common width fixed to 0.15 GeV and with central values indicated by the arrows. The dashed curve shows the fitted background. The shaded histogram is from the normalized ω mass sideband events and the cross-hatched histogram shows the normalized continuum contributions.

with different $G_{0^{--}}$ widths from 0.0 to 0.5 GeV in steps of 0.05 GeV are listed in Table II. The results are displayed graphically in Fig. 17.

VI. SYSTEMATIC ERRORS

Several sources of systematic errors are taken into account in the branching fraction measurements. The systematic uncertainty of 0.35% per track due to charged-track reconstruction is determined from a study of partially reconstructed $D^{*+} \rightarrow D^0(\rightarrow K_S^0\pi^+\pi^-)\pi^+$ decays. It is additive. The photon reconstruction contributes 2.0% per photon, as determined using radiative Bhabha
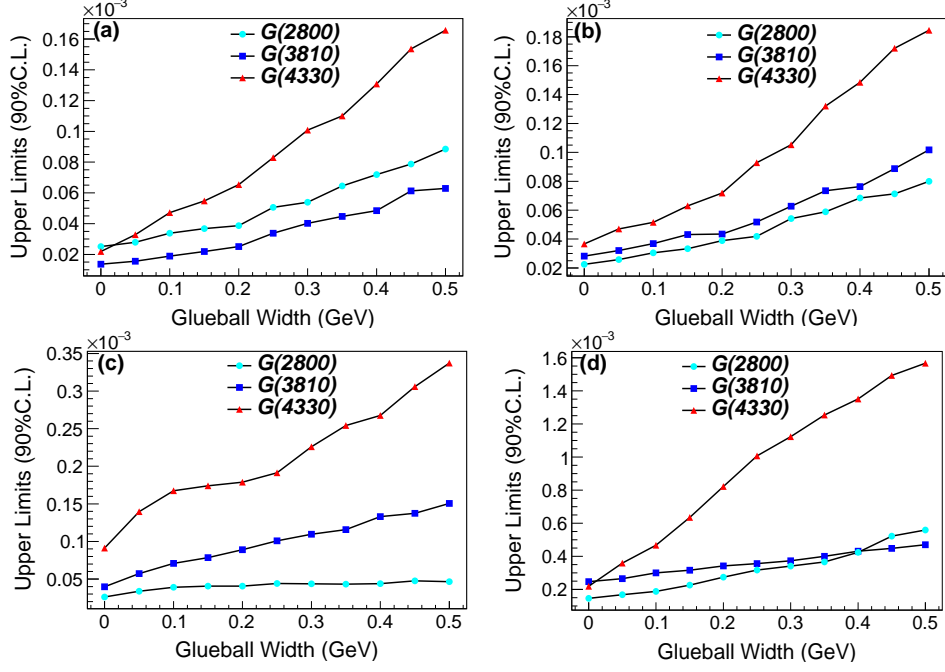
FIG. 17: (Color online) The upper limits on the branching fractions for $\Upsilon(1S) \to f_1(1285) + G_{0--}$ (a), $\Upsilon(2S) \to f_1(1285) + G_{0--}$ (b), $\chi_{b1} \to J/\psi + G_{0--}$ (c), and $\chi_{b1} \to \omega + G_{0--}$ (d) as a function of the assumed G_{0--} decay width.

events. Based on the measurements of the particle identification efficiencies of lepton pairs from $\gamma\gamma \to \ell^+\ell^-$ events and pions from a low-background sample of D^* events, the MC simulation yields uncertainties of 3.6% for each lepton pair and 1.3% for each pion. The MC statistical errors are estimated using the numbers of selected and generated events; these are 1.0% or less. The trigger efficiency evaluated from simulation is approximately 100% with a negligible uncertainty. Errors on the branching fractions of the intermediate states are taken from Ref. [20]. The uncertainties of the branching fractions of $\Upsilon(2S) \to \gamma\chi_{b1}$, $\chi_{c1} \to \gamma J/\psi$, $J/\psi \to \ell^+\ell^-$, $f_1(1285) \to a_0(980)\pi$, $\eta \to \gamma\gamma$, $\omega \to \pi^+\pi^-\pi^0$ and $\pi^0 \to \gamma\gamma$ are 5.8%, 3.5%, 1.1%, 19.4%, 0.5%, 0.8% and 0.04%, respectively. By changing the order of the background polynomial and the range of the fit, the decay-dependent relative difference in the upper limits of the number of signal events is obtained; this is taken as the systematic error due to the uncertainty of the fit. Finally, the uncertainties on the total numbers of $\Upsilon(1S)$ and $\Upsilon(2S)$ events are 2.2% and 2.3%, respectively, which are mainly due to imperfect simulations of the charged-track multiplicity distributions from inclusive hadronic MC events. Assuming that all of these systematic-error sources are independent, the total systematic errors are summed in quadrature and listed in Table II for all the studied modes under the assumptions of different G_{0--} widths.

20

VII. RESULTS AND DISCUSSION

In summary, using the large data samples of 102×10^6 $\Upsilon(1S)$ and 158×10^6 $\Upsilon(2S)$ events collected by the Belle detector, we have searched for the 0^{--} glueball in $\Upsilon(1S)$, $\Upsilon(2S)$, and χ_{b1} decays for the first time. No evident signal is found at three theoretically-predicted masses in the processes $\Upsilon(1S, 2S) \rightarrow \chi_{c1} + G_{0--}$, $\Upsilon(1S, 2S) \rightarrow f_1(1285) + G_{0--}$, $\chi_{b1} \rightarrow J/\psi + G_{0--}$, and $\chi_{b1} \rightarrow \omega + G_{0--}$ and 90% C.L. upper limits are set on the branching fractions for these processes. Figures 8 and 17 show the upper limits on the branching fractions as a function of the 0^{--} glueball width. The results presented in this article do not strongly depend on the spin-parity assumption of the glueballs. We also scan with fits across the mass regions up to 6.0 GeV/c^2 for all of the modes under study. All the signal significances are less than 3σ except for $\Upsilon(1S) \rightarrow f_1(1285) + G_{0--}$, where the maximum signal significance is 3.7σ at 3.92 GeV/c^2. It should be noted that we report here the local statistical significances without considering the look-elsewhere effect, which will largely reduce the significances. As we do not observe signals in any of the modes under study, the upper limits can be applied almost directly to the glueballs in this mass region with the same width and opposite spin parity and charge-conjugate parity, such as $J^{PC} = (0, 1, 2, 3)^{+-}$ and $(1, 2, 3)^{--}$ [23]. In addition, distinct χ_{c1} signals are observed in the $\Upsilon(1S)$ and $\Upsilon(2S)$ inclusive decays. The corresponding branching fractions are measured to be $\mathcal{B}(\Upsilon(1S) \rightarrow \chi_{c1} + anything) = (1.90 \pm 0.43(stat.) \pm 0.14(syst.)) \times 10^{-4}$ with substantially improved precision compared to the previous result of $(2.3 \pm 0.7) \times 10^{-4}$ [19], and $\mathcal{B}(\Upsilon(2S) \rightarrow \chi_{c1} + anything) = (2.24 \pm 0.44(stat.) \pm 0.20(syst.)) \times 10^{-4}$, measured for the first time.

---

[1] R. L. Jaffe and K. Johnson, Phys. Lett. B **60**, 201 (1976).

[2] C. F. Qiao and L. Tang, Phys. Rev. Lett. **113**, 221601 (2014).

[3] L. Bellantuono, P. Colangelo and F. Giannuzzi, J. High Energy Phys. **1510**, 137 (2015).

[4] C. P. Shen *et al.* (Belle Collaboration), Phys. Rev. D **88**, 011102(R) (2013).

[5] A. Abashian *et al.* (Belle Collaboration), Nucl. Instr. and Methods Phys. Res. Sect. A **479**, 117 (2002).

[6] J. Brodzicka *et al.*, Prog. Theor. Exp. Phys. (2012) 04D001.

[7] S. Kurokawa and E. Kikutani, Nucl. Instr. and Methods Phys. Res. Sect. A **499**, 1 (2003), and other papers included in this volume.

[8] T. Abe *et al.*, Prog. Theor. Exp. Phys. (2013) 03A001 and following articles up to 03A011.

[9] D. J. Lange, Nucl. Instr. and Methods Phys. Res. Sect. A **462**, 152 (2001).

[10] K. W. Edwards *et al.* (CLEO Collaboration), Phys. Rev. D **59**, 032003 (1999).

[11] T. Sjostrand, S. Mrenna and P. Skands, J. High Energy Phys. **05**, 026 (2006).

[12] E. Nakano, Nucl. Instr. and Methods Phys. Res. Sect. A **494**, 402 (2002).

[13] K. Hanagaki *et al.*, Nucl. Instr. and Methods Phys. Res. Sect. A **485**, 490 (2002).

[14] A. Abashian *et al.*, Nucl. Instr. and Methods Phys. Res. Sect. A **491**, 69 (2002).

[15] V. M. Aulchenko *et al.*, (KEDR Collaboration), Phys. Rett. B **573**, 63 (2003).

[16] K. Y. Liu, Z. G. He and K. T. Chao, Phys. Rev. D **69**, 094027 (2004).

[17] F. Yuan, C. F. Qiao and K. T. Chao, Phys. Rev. D **56**, 321 (1997).

[18] K. T. Chao, Z. G. He, D. Li and C. Meng, arXiv:1310.8597 [hep-ph]; C. Meng (private communication).

[19] R. A. Briere *et al.* (CLEO Collaboration), Phys. Rev. D **70**, 072001 (2004).

[20] K. A. Olive *et al.* (Particle Data Group), Chin. Phys. C **38**, 090001 (2014).

[21] The Novosibirsk function is defined as $f(x) = \exp[-\frac{1}{2}(\ln^2(1 + \Lambda(x - x_0))/\tau^2 + \tau^2)]$ with $\Lambda = \sinh(\tau\sqrt{\ln 4})/(\sigma\sqrt{\ln 4})$. The parameters represent the mean (x_0), the width (σ) and the tail asymmetry (τ).

[22] In common high-energy physics usage, this Bayesian interval has been reported as "confidence interval," which is a frequentist-statistics term.

[23] Y. Chen *et al.*, Phys. Rev. D **73**, 014516 (2006).

TABLE II: Summary of the upper limits for $\Upsilon(1S, 2S) \to \chi_{c1} + G_{0--}$, $f_1(1285) + G_{0--}$, and $\chi_{b1} \to J/\psi + G_{0--}$, $\omega + G_{0--}$ under different assumptions of G_{0--} width (Γ in GeV), where N^{UL} is the upper limit on the number of signal events taking into account systematic errors, ε is the reconstruction efficiency, σ_{syst} is the total systematic uncertainty and $\mathcal{B}^{\mathrm{UL}}$ is the 90% C.L. upper limit on the branching fraction.

	$\Upsilon(1S) \to \chi_{c1} + G(2800)/G(3810)/G(4330)$				$\Upsilon(2S) \to \chi_{c1} + G(2800)/G(3810)/G(4330)$			
Γ	N^{UL}	$\varepsilon(\%)$	$\sigma_{\mathrm{syst}}(\%)$	$\mathcal{B}^{\mathrm{UL}}(\times 10^{-6})$	N^{UL}	$\varepsilon(\%)$	$\sigma_{\mathrm{syst}}(\%)$	$\mathcal{B}^{\mathrm{UL}}(\times 10^{-6})$
0.00	5.5/4.4/9.2	19.9/24.6/26.3	6.6/10.8/7.6	6.8/4.5/8.8	12.9/6.9/11.3	19.7/24.6/25.6	6.6/15.9/8.6	10.6/4.4/7.3
0.05	6.1/5.6/11.1	19.5/25.1/26.5	6.7/8.1/9.6	7.8/5.3/10.6	14.7/8.2/16.6	19.2/24.7/25.6	6.7/14.2/16.4	12.7/5.5/10.8
0.10	6.8/7.0/13.3	20.2/24.6/26.0	7.1/7.2/11.4	8.6/7.2/13.0	16.2/9.5/23.7	19.8/24.5/25.2	7.0/16.8/21.5	13.5/6.4/15.6
0.15	7.3/9.9/15.2	20.1/25.0/26.4	7.3/6.3/12.9	9.1/10.0/14.6	16.9/10.9/30.6	19.6/24.5/26.0	7.4/18.9/21.8	14.4/7.3/19.6
0.20	7.6/11.6/17.2	19.8/25.0/25.9	7.3/6.3/13.9	9.8/11.8/16.8	17.0/11.8/38.4	19.7/24.0/25.2	7.6/20.6/27.1	14.4/8.0/25.8
0.25	8.5/14.5/21.4	19.6/24.5/26.4	7.4/6.3/16.5	10.9/15.1/20.6	18.7/14.6/47.1	18.8/24.0/25.6	8.6/23.8/28.4	16.6/10.0/30.6
0.30	8.7/16.3/24.9	18.9/24.4/26.6	6.7/6.5/16.2	11.6/17.0/23.8	20.6/16.5/54.9	18.6/23.8/25.7	11.4/26.4/29.7	18.4/11.5/34.9
0.35	8.9/19.3/28.2	19.6/24.3/26.6	6.3/7.2/19.8	11.8/20.0/26.8	20.1/18.0/62.5	18.8/23.7/25.6	12.5/27.3/34.2	17.8/12.5/39.9
0.40	9.0/21.8/29.7	19.2/24.8/26.3	10.3/7.3/20.3	12.0/22.3/28.7	21.4/21.3/75.7	18.6/24.2/25.8	9.2/31.0/42.3	19.0/14.6/48.9
0.45	9.2/22.7/32.3	19.2/24.3/26.4	10.1/7.5/21.2	12.2/23.7/31.1	21.5/22.2/85.6	18.8/23.9/25.2	9.9/31.7/44.4	19.1/15.5/56.5
0.50	9.6/24.2/36.8	19.4/24.8/26.8	7.7/8.1/22.7	12.5/24.7/35.0	22.4/24.1/103.7	18.7/24.0/25.9	11.7/33.0/47.8	19.9/16.6/66.8

	$\Upsilon(1S) \to f_1(1285) + G(2800)/G(3810)/G(4330)$				$\Upsilon(2S) \to f_1(1285) + G(2800)/G(3810)/G(4330)$			
Γ	N^{UL}	$\varepsilon(\%)$	$\sigma_{\mathrm{syst}}(\%)$	$\mathcal{B}^{\mathrm{UL}}(\times 10^{-5})$	N^{UL}	$\varepsilon(\%)$	$\sigma_{\mathrm{syst}}(\%)$	$\mathcal{B}^{\mathrm{UL}}(\times 10^{-5})$
/ 0.00	23.0/19.5/33.0	8.3/9.9/10.4	22.5/22.4/23.0	2.5/1.4/2.2	38.6/61.1/83.4	7.7/9.7/10.2	20.5/22.4/22.1	2.2/2.8/3.7
0.05	33.4/22.4/49.7	8.3/9.9/10.5	22.7/21.0/25.2	2.8/1.6/3.3	45.1/69.8/107.3	7.8/9.7/10.2	20.7/20.4/23.2	2.6/3.2/4.7
0.10	40.3/26.9/70.5	8.2/9.8/10.3	23.3/24.7/28.3	3.4/1.9/4.7	53.6/80.1/118.6	7.8/9.7/10.2	20.9/21.1/25.0	3.1/3.7/5.2
0.15	43.0/31.6/83.0	8.1/10.0/10.5	24.0/31.5/29.5	3.7/2.2/5.5	58.6/92.4/143.2	7.8/9.6/10.1	21.0/21.4/24.3	3.3/4.3/6.3
0.20	45.7/35.8/97.2	8.2/9.9/10.3	24.4/33.6/32.5	3.9/2.5/6.5	68.2/92.8/165.5	7.8/9.5/10.3	21.2/22.0/24.6	3.9/4.3/7.2
0.25	59.8/48.0/123.6	8.2/9.8/10.3	26.4/27.5/34.4	5.1/3.4/8.8	73.4/110.7/213.3	7.8/9.5/10.2	21.4/22.6/25.3	4.2/5.2/9.3
0.30	63.4/57.1/152.3	8.1/9.8/10.4	26.8/25.4/35.9	5.4/4.0/10.0	95.0/134.2/239.4	7.8/9.6/10.1	21.9/21.7/25.7	5.4/6.3/10.5
0.35	74.8/63.3/163.7	8.0/9.8/10.3	27.7/22.5/36.8	6.5/4.5/11.0	101.3/156.9/299.2	7.7/9.5/10.1	22.1/21.2/25.6	5.9/7.3/13.2
0.40	82.1/68.3/195.1	7.9/9.7/10.3	29.3/22.2/36.8	7.2/4.9/13.1	119.6/165.8/337.5	7.8/9.7/10.1	22.7/20.4/25.6	6.8/7.6/14.8
0.45	90.4/86.5/229.4	7.9/9.7/10.3	30.2/20.3/38.5	7.9/6.1/15.4	120.4/187.4/388.4	7.5/9.4/10.1	22.7/23.2/26.0	7.1/8.9/17.2
0.50	103.8/89.1/248.1	8.1/9.8/10.3	30.4/23.0/38.7	8.8/6.3/16.6	135.8/214.6/416.3	7.6/9.4/10.1	23.3/22.5/26.0	8.0/10.2/18.4

	$\chi_{b1} \to J/\psi + G(2800)/G(3810)/G(4330)$				$\chi_{b1} \to \omega + G(2800)/G(3810)/G(4330)$			
Γ	N^{UL}	$\varepsilon(\%)$	$\sigma_{\mathrm{syst}}(\%)$	$\mathcal{B}^{\mathrm{UL}}(\times 10^{-5})$	N^{UL}	$\varepsilon(\%)$	$\sigma_{\mathrm{syst}}(\%)$	$\mathcal{B}^{\mathrm{UL}}(\times 10^{-4})$
0.00	5.9/11.4/29.4	17.8/23.6/26.2	9.4/9.5/21.2	2.6/4.0/9.1	57.7/132.7/133.5	4.1/5.6/6.3	9.8/11.0/14.4	1.4/2.5/2.2
0.05	7.8/15.8/43.6	18.3/22.7/25.6	9.6/9.9/15.3	3.4/5.7/13.9	66.2/148.2/223.7	4.1/5.8/6.5	9.7/10.3/9.4	1.7/2.6/3.6
0.10	8.9/19.6/51.4	18.4/22.6/25.0	9.2/10.0/14.6	3.9/7.1/16.7	74.0/161.4/285.9	4.1/5.6/6.4	10.3/14.9/9.0	1.8/3.0/4.7
0.15	9.3/22.3/55.6	18.2/23.1/26.2	9.2/8.3/13.6	4.0/7.9/17.4	91.1/166.6/384.5	4.2/5.5/6.3	9.8/19.1/8.5	2.2/3.2/6.3
0.20	9.5/25.5/56.6	18.5/23.4/25.9	9.2/7.8/13.0	4.1/8.9/17.8	110.0/178.6/494.9	4.2/5.4/6.2	9.7/20.2/12.3	2.7/3.4/8.2
0.25	9.7/29.8/60.8	18.0/24.1/25.9	8.3/7.8/12.7	4.2/10.1/19.1	119.5/185.7/603.9	4.0/5.4/6.2	9.4/20.9/9.3	3.2/3.6/10.1
0.30	9.8/31.9/71.5	17.8/23.8/25.9	9.3/8.0/13.1	4.3/10.9/22.6	131.9/200.3/686.3	4.0/5.6/6.4	9.9/22.0/10.8	3.4/3.7/11.2
0.35	9.9/34.0/77.9	18.2/24.0/25.1	10.8/8.1/14.0	4.4/11.6/25.4	144.6/210.8/761.1	4.1/5.5/6.3	10.8/19.7/8.9	3.6/4.0/12.5
0.40	9.9/38.6/83.5	18.0/23.7/25.5	9.2/8.5/13.4	4.5/13.3/26.7	164.1/226.4/814.8	4.0/5.4/6.3	11.6/17.2/17.7	4.2/4.3/13.5
0.45	10.3/38.9/95.5	17.8/23.2/25.6	8.9/8.5/13.6	4.6/13.7/30.6	201.9/235.6/906.0	4.0/5.4/6.3	11.8/16.1/10.4	5.2/4.5/14.9
0.50	10.4/42.9/105.1	18.1/23.3/25.5	10.1/8.5/14.0	4.7/15.0/33.7	209.0/244.4/983.7	3.9/5.4/6.5	11.6/11.7/9.3	5.6/4.7/15.7